ADVANCED FUNCTIONAL MATERIALS
www.afm-journal.de

Thermally Stable Silver Nanowire–Polyimide Transparent Electrode Based on Atomic Layer Deposition of Zinc Oxide on Silver Nanowires

*Dustin Chen, Jiajie Liang, Chao Liu, Gillian Saldanha, Fangchao Zhao, Kwing Tong, Jiang Liu, and Qibing Pei**

The performance of a flexible transparent conductive electrode with extremely smooth topography capable of withstanding thermal processing at 300 °C for at least 6 h with little change in sheet resistance and optical clarity is reported. In depth investigation is performed on atomic layer deposition (ALD) deposited ZnO on Ag nanowires (NWs) with regard to thermal and atmospheric corrosion stability. The ZnO coated nanowire networks are embedded within the surface of a polyimide matrix, and the <2 nm roughness freestanding electrode is used to fabricate a white polymer light emitting diode (PLED). PLEDs obtained using the ZnO-AgNW-polyimide substrate exhibit comparable performance to indium tin oxide (ITO)/glass based devices, verifying its efficacy for use in optoelectronic devices requiring high processing temperatures.

1. Introduction

Transparent conductive electrodes (TCEs) are critical components in optoelectronic devices, and can be found in devices ranging from touch sensors, display technology, to organic light emitting diodes (OLEDs).[1] The current industry standard for TCEs is indium tin oxide (ITO), which has been ubiquitous for most practical thin-film transparent electrode applications over the course of the past several decades.[2] However, ITO is expensive due to the scarcity of indium, there are potential health issues due to the exposure of indium based powders,[3] and ITO films are brittle and the underlying glass substrate thick, restricting their use for flexible optoelectronic devices.[4] These inherent drawbacks of ITO necessitate the development of alternative TCEs for next generation optoelectronic devices. In the selection for TCEs, the two critical requirements most commonly discussed are high conductivity and transparency, seemingly contradictory as these two parameters vary inversely with film thickness.[5]

Leading candidates for TCEs that satisfy these requirements include carbon based materials such as carbon nanotube (CNT)[6,7] and graphene,[8,9] metal grids,[1,10] and networks of metallic nanowires.[11,12] Though promising candidates, carbon nanostructured based materials do not have the combined transparency and conductivity requirement necessitated for optoelectronic applications such as solar cells and OLEDs, and metal nanogrids require expensive batch based processing, making them impractical for large scale applications.[1] In comparison, metal-based nanowires such as silver nanowires (AgNW) networks have desirable electrical, mechanical, and optical properties, in addition to being solution processed, allowing for high speed, low cost, roll-to-roll processing.

Despite significant advantages over leading competitors, AgNW films still suffer from inherent drawbacks, most notably the rough surface topology and poor thermal stability of the AgNW composite electrode.[13] Several attempts at ameliorating these issues have been reported, though a solution simultaneously resolving both the aforementioned problems has not yet surfaced. Embedding the AgNW layer within the polymer has been shown to drastically reduce the surface roughness,[13–18] which can prevent short circuits that can lead to device failure. With this technique, a glass substrate is typically used to provide a smooth release for the AgNW infused with polymer, yielding surface roughnesses below 2 nm.[14] To improve thermal stability, polymers with a higher glass transition temperature (T_g) such as polyimide, or reinforced hybrid polymers have been used.[13,15–17,19] As an example, one of our previous works used AgNWs inlaid in the surface of a heat-resistant acrylate matrix to be used as a thin film heater, though the device was only tested at a maximum temperature of 230 °C for time scales under 5 min.[17] However, TCEs with thermally stable polymer matrices do not account for the thermal stability of the AgNW themselves, which exhibit an increase in sheet resistance at 180 °C when the nanowires are freestanding, and often at even lower temperatures when embedded in a polymer matrix.[20] This increase of resistivity is due to nanoscale size effects, causing NWs to melt at a significantly lower temperature than the melting temperature of bulk silver.[21] A sandwich layer of zinc oxide (ZnO)/AgNW/ZnO has been shown to increase the thermal stability of the silver nanowires,[19,22,23] but the continuous layer of ZnO over the AgNW film prohibit the infiltration of a polymer precursor to form a percolation network, leading to a high surface roughness which

D. Chen, Dr. J. Liang, C. Liu, G. Saldanha,
Dr. F. Zhao, K. Tong, Dr. J. Liu, Prof. Q. Pei
Department of Materials Science and Engineering
Henry Samueli School of Engineering and Applied Science
University of California
Los Angeles, CA 90095, USA
E-mail: qpei@seas.ucla.edu

DOI: 10.1002/adfm.201503236

cause shorts and device failure. Chen et al. used stamp-transferred graphene on AgNW to allow graphene to dissipate heat in order to protect the AgNWs, but were only able to maintain stability at 200 °C for 3 h, in addition to not fabricating freestanding films.[21] The use of neutral-pH poly(3,4-ethylenedioxythiophene): poly(styrenesulfonate) (PEDOT:PSS) was reported to improve thermal stability of the AgNW electrode, but could only withstand 20 min annealing at 210 °C due to the degradation of PEDOT:PSS at high temperatures.[24]

Here, we report on the use of a low temperature atomic layer deposition (ALD) process to coat a conformal, thin layer of ZnO around individual nanowires to enhance the thermal stability of AgNWs while maintaining a porous structure. ALD on AgNW has been shown to improve the stability of AgNW,[25,26] albeit no reports on the long term thermal stability have been conducted, and freestanding films have not been fabricated. Thermally stable and colorless polyimide (PI) was chosen as the polymer matrix to embed the coated AgNWs. The resulting composite electrode successfully resolves the issue of thermal stability for both the AgNWs and polymer matrix, while still embedding the AgNW within the polymer matrix for low surface roughness. The composite sheets show high long-term thermal stability up to 300 °C, mechanical flexibility, resistance to atmospheric corrosion, and outperform ITO/polyethylene terephthalate (PET), a common transparent flexible electrode, in visual transparency, surface conductivity, and surface smoothness. The efficacy of the new ZnO-AgNW-PI TCE was demonstrated by solution-processing polymer LEDs (PLEDs), with the ZnO-AgNW-PI TCE having performance comparable to ITO, and vastly outperforming control noncoated AgNW based TCEs.

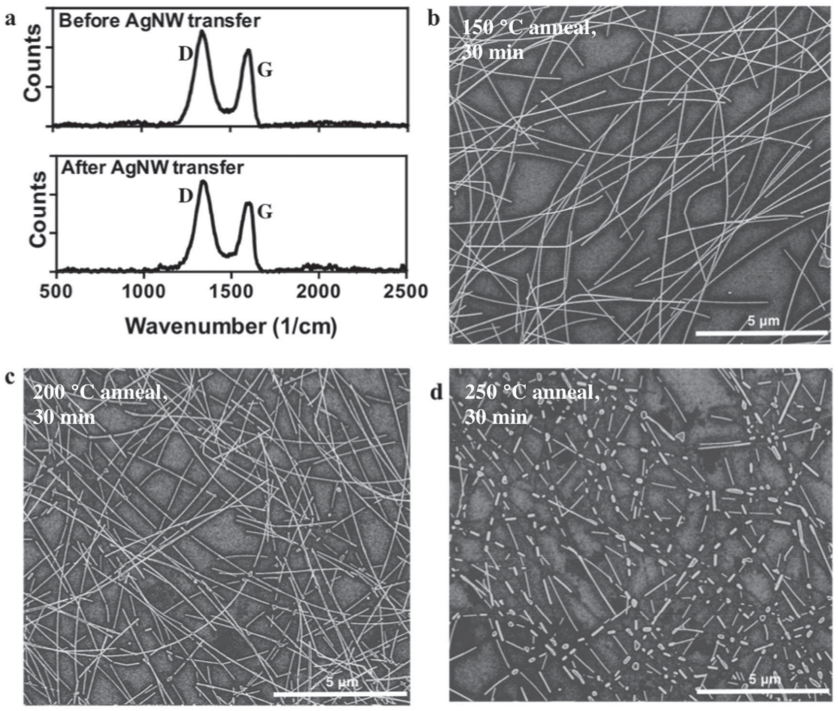

Figure 1. a) Raman spectra of the GO-coated glass release substrate before (top) and after (bottom) PI transfer of ZnO-AgNW film. b) AgNW bar coated on a glass slide after a 150 °C anneal for 30 min. c) AgNW coated on a glass substrate after a 200 °C anneal for 30 min. d) AgNW coated on a glass substrate after a 250 °C anneal for 30 min.

2. Results and Discussion

Fabrication of the porous electrode network was achieved by drawing down liquid solution with a Mayer rod onto a release glass substrate. First, a solution of graphene oxide (GO) was drawn down to act as a sacrificial layer when transferring the AgNW to PI matrix. **Figure 1**a illustrates the Raman spectra before and after the transfer process to confirm the presence of GO with the same Raman intensity. The characteristic D and G bands of graphene oxide[27] are present before and after transferring both pristine AgNW and ZnO-AgNW, confirming its use as a sacrificial layer. Following GO coating, a AgNW network was coated to a sheet resistance (R_{sh}) of 10 Ω sq^{-1} and 91% transparency. The solution-processed electrode on glass was subsequently brought into an ALD chamber for low temperature thermal deposition. Because ALD deposition relies exclusively on surface reactions, with hydroxylated surfaces typically being the most reactive with ALD precursors, a thin layer of aluminum oxide (Al_2O_3) was deposited as an adhesive layer prior to ZnO deposition. Al_2O_3 was selected as the adhesive layer as its precursor, trimethyl aluminum (TMA), has been shown to react well with Ag and provides a hydroxylated surface for subsequent deposition processes.[26,28] ZnO was deposited immediately following Al_2O_3. Both materials were deposited using a low temperature thermal deposition process to prevent oxidation and melting of the AgNWs.

ZnO coated and pristine AgNW electrodes were heated at 150, 200, and 250 °C for 30 min to verify the stability of the electrodes at high temperatures. It has been reported that at temperatures above 180 °C, a sharp increase in R_{sh} is observed due to the coalescence of the nanowires into discrete droplets and the formation of a thin oxide layer that decrease electrical performance.[13,20] While both pristine (Figure 1b) and ZnO coated AgNWs were found to remain intact in a percolating network at 150 °C, the beginning of coalescence into isolated droplets and fragmented nanowires were observed at 200 °C (Figure 1c), and complete conversion of nanowires into discrete Ag nanoparticles at 250 °C for pristine AgNWs, as seen in Figure 1d.

The coating of AgNW with ZnO was expected to greatly enhance the thermal stability of the electrodes. The melting temperature of bulk ZnO greatly exceeds that of silver, with the T_m for the metal oxide approaching 2000 °C.[29] When accounting for melting point depression brought about by the size effects, the melting point of ZnO nanostructures with radii under 10 nm still exceed 1000 °C,[29] well over the processing temperatures required for OLED processing. To verify the enhanced thermal stability of the electrodes endowed by the

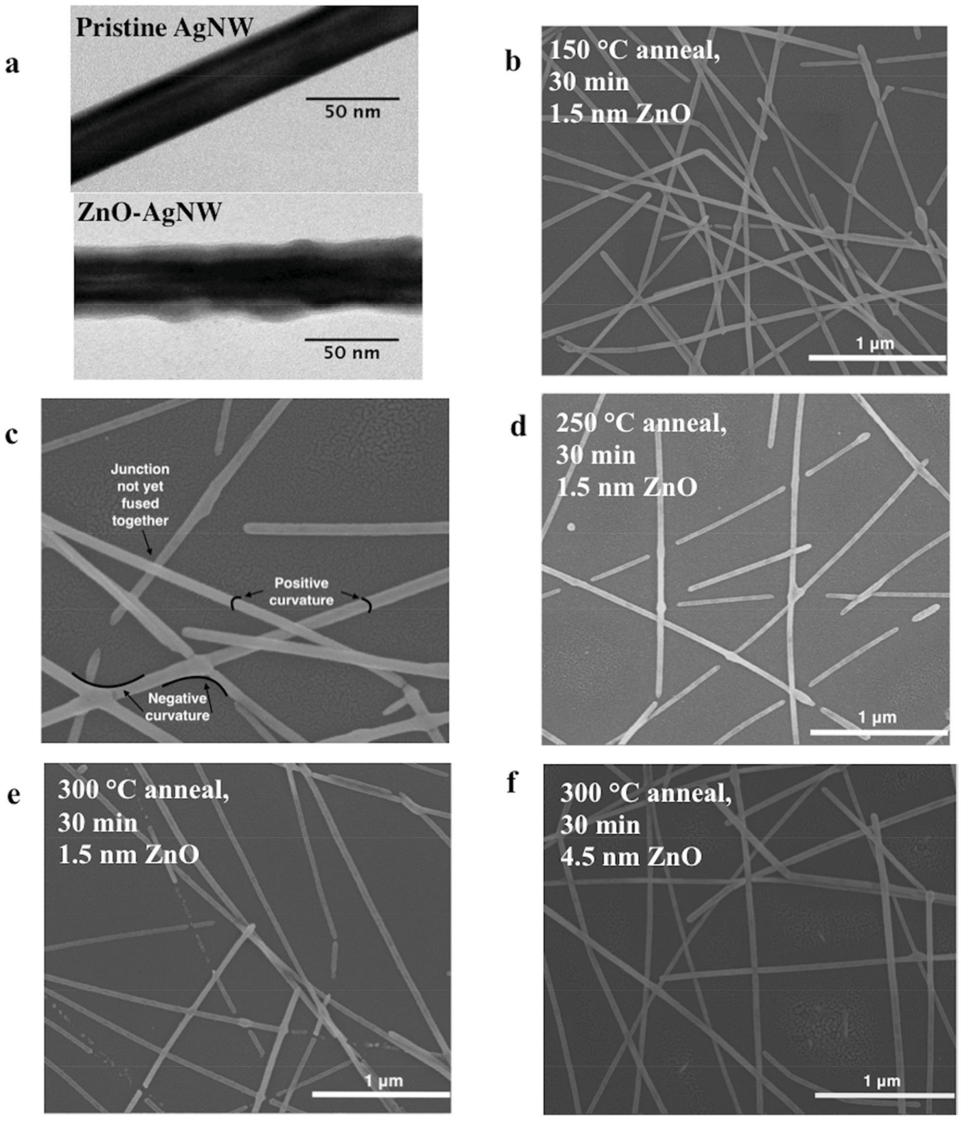

Figure 2. a) TEM image of pristine (top), and ZnO coated AgNW (bottom). b) SEM image of ZnO-coated AgNW on glass substrate without annealing. c) SEM image illustrating positive and negative curvatures. d) SEM image of 1.5 nm of ZnO-AgNW after a 250 °C anneal for 30 min. e) SEM image of 1.5 nm ZnO-AgNW after a 300 °C anneal for 30 min. f) SEM image of 4.5 nm ZnO-AgNW after a 300 °C anneal for 30 min.

ZnO coating, AgNW samples were coated with 1.0, 1.5, 3, 4.5, 6, and 7.5 nm of ZnO, and subsequently annealed at temperatures between 200 and 300 °C. The resulting electrodes were analyzed with SEM imaging to determine the minimum thickness of ZnO at which the additional thermal stability afforded to the AgNW remained intact. Silver was sputtered onto glass slides to be used as a reference before being brought into the ALD chamber to concurrently deposit ZnO on the reference and AgNW films, and the thicknesses of the ZnO layers were subsequently measured using a FilmTek 2000 ellipsometer. Transmission electron microscopy (TEM) images of AgNWs with and without ZnO are shown in **Figure 2**a to illustrate the ZnO wrapping completely around the AgNW. A sample with 7.5 nm ZnO thickness measured with ellipsometry was imaged, matching well with the 7.8 nm measured from TEM. Though the bare AgNW shown is thicker than the ZnO coated AgNW, with different thicknesses of nanowires evident in SEM imaging as well (Figure 2b), the ability to coat the desired ALD thickness on different dimension nanowires highlights the efficacy of this approach.

Standridge et al. conducted a study of ALD deposited TiO_2 on AgNW and found that below a certain thickness threshold, the resulting incomplete coverage of TiO_2 lead to significantly enhanced etching rates when placed in corrosive I^-/I_3^- solutions.[26] Similarly, it is hypothesized that below a certain thickness threshold for ZnO, incomplete coverage would enable the underlying Ag to melt and reform as discrete Ag droplets. While no samples showed adverse effects of annealing at 200 °C, the beginning of junction deterioration was observed for samples with a ZnO thickness below 3 nm when annealed at 250 °C. The melting and coalescence at the junction is believed to be caused in part by incomplete coverage of the protective

ZnO coating at very low thicknesses. Because the AgNW film is comprised of layers of AgNWs stacked on top of each other, the bottom layers may not be exposed to precursor flow for long enough periods to render complete coverage, similar to high aspect nanostructures experiencing thinning regions in deeper portion of the nanostructure.[30,31] In addition, the nanowires experience higher localized temperature at the junctions between individual nanowires. According to the Gibbs–Thomson theory, $\Delta G = \gamma \Omega r^{-1}$, where ΔG is the change in Gibbs Thomson potential, γ is the surface energy, Ω is the volume per atom, and r is the radius, the Gibbs–Thomson potential is inversely related to the radius of the nanowire. At the junction between nanowires, a negative curvature is present, leading to a negative value of the Gibbs–Thomson potential, as illustrated in Figure 2c. However, the radius of individual nanowires is positive, leading to a positive Gibbs–Thomson potential, and thus, a large potential difference between the junction and regions immediately adjacent to the junction. This large potential gradient is a driving force for diffusion, causing the migration of atoms into the junction, which, over time, leads to the fragmentation of nanowires close to the junction. This phenomenon is clearly observed through the enlarged area around certain junctions, in addition to the discontinuity of select nanowires immediately adjacent to junctions as shown in Figure 2d.

At samples heated to 300 °C, partial coalescence of nanowires into droplets for samples with a ZnO thickness below 1.5 nm is observed. Again from the Gibbs–Thomson equation, it is known that the melting point of a nanowire is related to the radius of the nanowire.[32,33] More specifically, the melting point of nanoparticles decreases with lower dimensions. In Figure 2e, the formation of Ag nanoparticles is evident in nanowires with shorter radii. In comparison, Figure 2f shows a 4.5 nm ZnO coated AgNW film annealed at 300 °C for 30 min with no significant fragmentation or coalescence of the nanowires.

In the selection of the optimal thickness of ZnO, the effect of the ZnO thicknesses on transparency and conductivity of the AgNW based electrode was analyzed. Figure S1 (Supporting Information) illustrates the transparency of AgNW electrodes before and after deposition of 1.5, 3.0, 4.5, and 7.5 nm ZnO. The transparency before and after ZnO deposition was virtually unchanged for all four samples with different thicknesses of ZnO. In addition, the sheet resistance of all samples remained essentially unchanged, with only variations below 1% observed when measuring sheet resistance before and after ZnO deposition. Thus, the selection of ZnO thickness was relegated to the lowest thickness of ZnO in which highly effective thermal protection was still present. It is important to note that even though the bulk of the nanowire networks remained intact after high temperature annealing even with low thicknesses of ZnO, remaining experiments were conducted using AgNW electrodes coated with 4.5 nm of ZnO to ensure optimal performance.

To quantitatively analyze the efficacy of the ALD coated AgNW film for high temperature processing, the sheet resistance and transmittance were evaluated and compared with pristine AgNWs before and after annealing. An electrical thermal stability test was performed by measuring the sheet resistance as a function of the annealing temperature to highlight the superior electrical performance of the ZnO-AgNW electrode. A ZnO-AgNW film coated on glass was annealed on an Instec

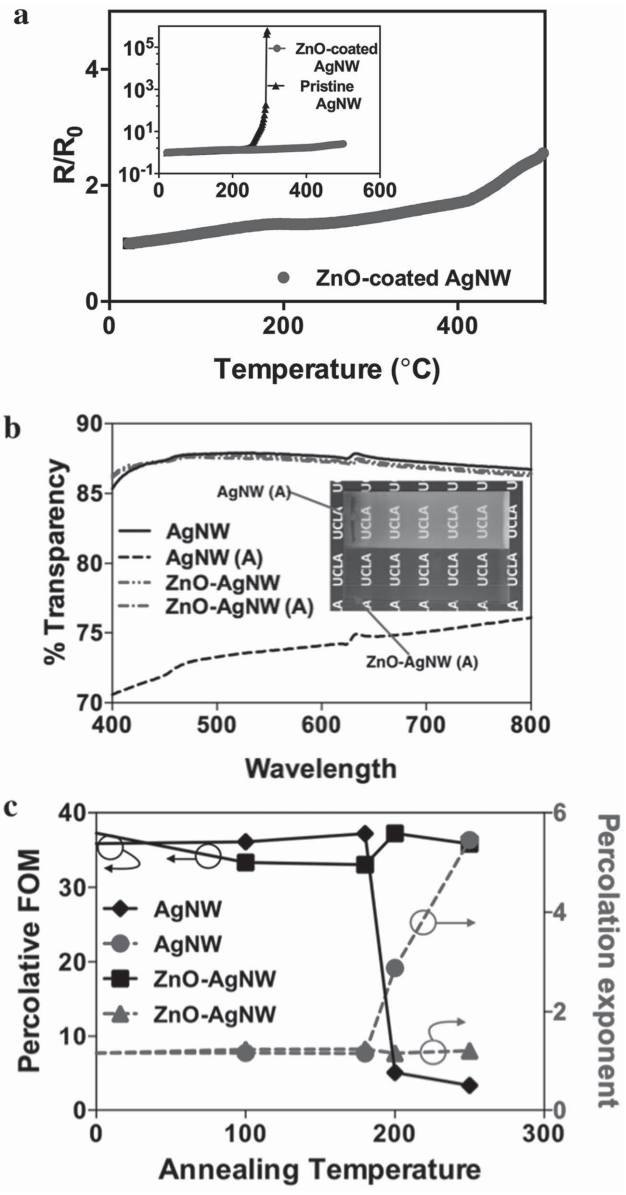

Figure 3. a) Normalized sheet resistance of ZnO-coated AgNW, with the normalized sheet resistance for ZnO-AgNW and pristine AgNW plotted on a logarithmic scale in the inset. b) UV–vis spectrum of annealed and nonannealed ZnO-coated AgNW films and pristine AgNW films (A) denotes annealed samples. c) Percolative figure of merit and percolation exponent as a function of annealing temperature for both ZnO-coated AgNW films and pristine AgNW films.

mK1000 high precision temperature controller with a ramp rate of 5 °C min^{-1}. The hot stage was sealed with a cover on top under ambient conditions to prevent heat loss from the surface sample due to convection. Two electrical leads were formed on the samples with silver paste, with connections leading outside of the testing stage to measure the sheet resistance in situ every 12 s. In the case of the pure AgNW film, an increase in sheet resistance deviating from the slight increase of resistance associated with increasing temperature in metals was observed, with a dramatic increase in R_{sh} beginning at 250 °C (**Figure 3**a). At temperatures above 300 °C, the sheet resistance exceeded

the maximum measuring limit of the voltmeter. The ZnO enhanced electrode showed only the expected slight continuous increase in resistance as a function of temperature, with no rapid increase in resistance up to 500 °C, at which the test was stopped due to the limitations of the instrument.

Though the poor electrical performance after high temperature annealing is largely attributed to the fragmentation of nanowires at temperatures above the melting point, atmospheric corrosion, primarily sulfidation and oxidation, which can occur at low temperatures, with increasingly deleterious effects with higher anneal temperatures, can also have detrimental effects for optoelectronic devices requiring high temperature processing.[34] The corroded AgNW films, in addition to increasing in sheet resistance, show significant transparency loss when compared to unannealed samples. In contrast, the ZnO-AgNW film exhibited excellent optical performance in the visible spectrum after annealing at 300 °C for 30 min, as seen in the inset of Figure 3b. Whereas the black background is clearly visible in the transparent ZnO coated electrode, the pristine AgNW sample subjected to the same annealing conditions is virtually fully opaque due to the atmospheric corrosion of silver by sulifdation and oxidation. Numerically, a 15% loss in transparency at 550 nm due to oxidation is observed in the noncoated AgNW when compared to noncoated, unannealed samples, as shown in Figure 3b. However, the ZnO coated nanowire showed no decrease in transparency after annealing in contrast to pristine, unannealed AgNWs, showing its efficacy in protecting the underlying AgNWs not only from melting, but oxidation as well. The optoelectronic performance can be compared between the AgNW and control sample through comparison of the percolative figure of merit and percolation exponent, two parameters often used in describing optoelectronic performance of metals nanowires.[35] These two parameters can be solved with the following equation[15,35]

$$T = \left[1 + \frac{1}{\Pi}\left(\frac{Z_0}{R_{sh}}\right)^{1/n+1}\right]^{-2} \quad (1)$$

where Π and n are the percolative figure of merit (PFOM) and percolation exponent (PE), respectively, T is the optical transmittance, and Z_0 is the impedance of free space (377 Ω). High values of Π and low values of n are conducive to higher performing optoelectronic performance for metal nanowire based TCEs. Six pairs of R_{sh} and T at each annealing temperature were used, and curve fitted to obtain the respective PFOM and PE. As can be seen in Figure 3c, the desirable trends for these two parameters are observed for ZnO-coated AgNW electrodes for different annealing temperatures, whereas a deterioration of the parameters is observed with higher annealing temperatures in the case of the pristine AgNWs.

To create freestanding electrodes for optoelectronic devices, the coated nanowire network were embedded and transferred from the glass substrate with a similar method reported in one of our previous publications, shown in **Figure 4**a.[14] Briefly, a PI solution was spun onto the ZnO-AgNW electrode, and then heated at 130 °C in a vacuum oven to remove excess solvent. A freestanding ZnO-AgNW-PI film of approximately 50 µm thickness was separated from the glass after solvent removal (Figure 4b). The embedding of the ZnO coated AgNW into the surface of the PI allows for a sub-2 nm R_a topography, as shown in Figure 4c, critical for the performance of certain optoelectronic devices such as OLEDs. Additional SEM images depicting the embedding of the AgNW within the polymer matrix are shown in Figure S2 (Supporting Information). Following separation of the ZnO-AgNW-PI electrode from glass, a bending test was conducted, flexing the electrode repeatedly to a 3.0 mm radius, as seen in Figure S3 (Supporting Information). During 5000 cycles of bending and unbending the resistance of the ZnO-AgNW-PI electrode remained stable, increasing in sheet resistance by less than 2%.

It is important to note that the very top of the freestanding electrode consist of a portion of AgNWs not coated with ZnO. This region of AgNWs is the portion of nanowires intimately in contact with the release glass substrate, preventing the infiltration of ALD precursors to coat the protective ZnO coating. However, this uncoated region comprises merely a small area of the AgNW surface. Figure S4 (Supporting Information) illustrates a SEM image of coated AgNWs on glass, highlighting the individual nanowires on the very bottom of the percolation network in contact with the glass. Because the percolation network consists of layers of AgNWs deposited on top of each other, only this very bottom layer consists of full nanowires intimately in contact with the glass, a fraction of the total nanowire network. Furthermore, of these bottom layer nanowires, less than 50% of the surface area actually will contact the release glass surface. Tilted SEM imaging of AgNWs show a relatively small area of nanowires actually pressed against the glass.[32] Because the mechanism of electrical decay with thermal annealing primarily consists of the fragmentation of the AgNWs into discrete nanoparticles, the partial, but majority coating of the bottom layer of nanowires is still sufficient to protect these nanowires. As the majority of the nanowires are fully coated, and the few that are not have coatings exceeding half of the surface area, the transferred AgNW network still exhibits high thermal stability.

To evaluate this thermal stability with regards to electrical and optical performance of the freestanding composite hybrid electrode, the sheet resistance of the as-prepared films was analyzed in situ with the mK 1000 high precision temperature controller, and UV–vis spectra were obtained before and after annealing. The efficacy of both thermally stable components, PI and ZnO, were evaluated by comparing the ZnO-AgNW-PI films with three control electrodes: a pristine AgNW-PI film, a ZnO-AgNW-acrylate film, and a AgNW-acrylate film. The acrylate utilized in the reference electrode was previously used for flexible PLED devices with enhanced light extraction in our previous publication.[14] ZnO-coated AgNW films were heated at 300 °C, for 6 h, while the reference films with pristine AgNW were heated to 250 °C also for 6 h, due to the inability of bare AgNWs to withstand higher temperatures. Regarding electrical stability, the AgNW-acrylate films failed in the first few minutes, with the resistance increasing over 10 MΩ, the limit of the voltmeter used to measure the resistance. Figure 4d shows the change in sheet resistance as a function of time for the two other reference electrodes, and the ZnO-AgNW-PI electrode. The AgNW-PI showed a linear increase in sheet resistance, with the final resistance after cooling back down to room temperature more than three times the original sheet

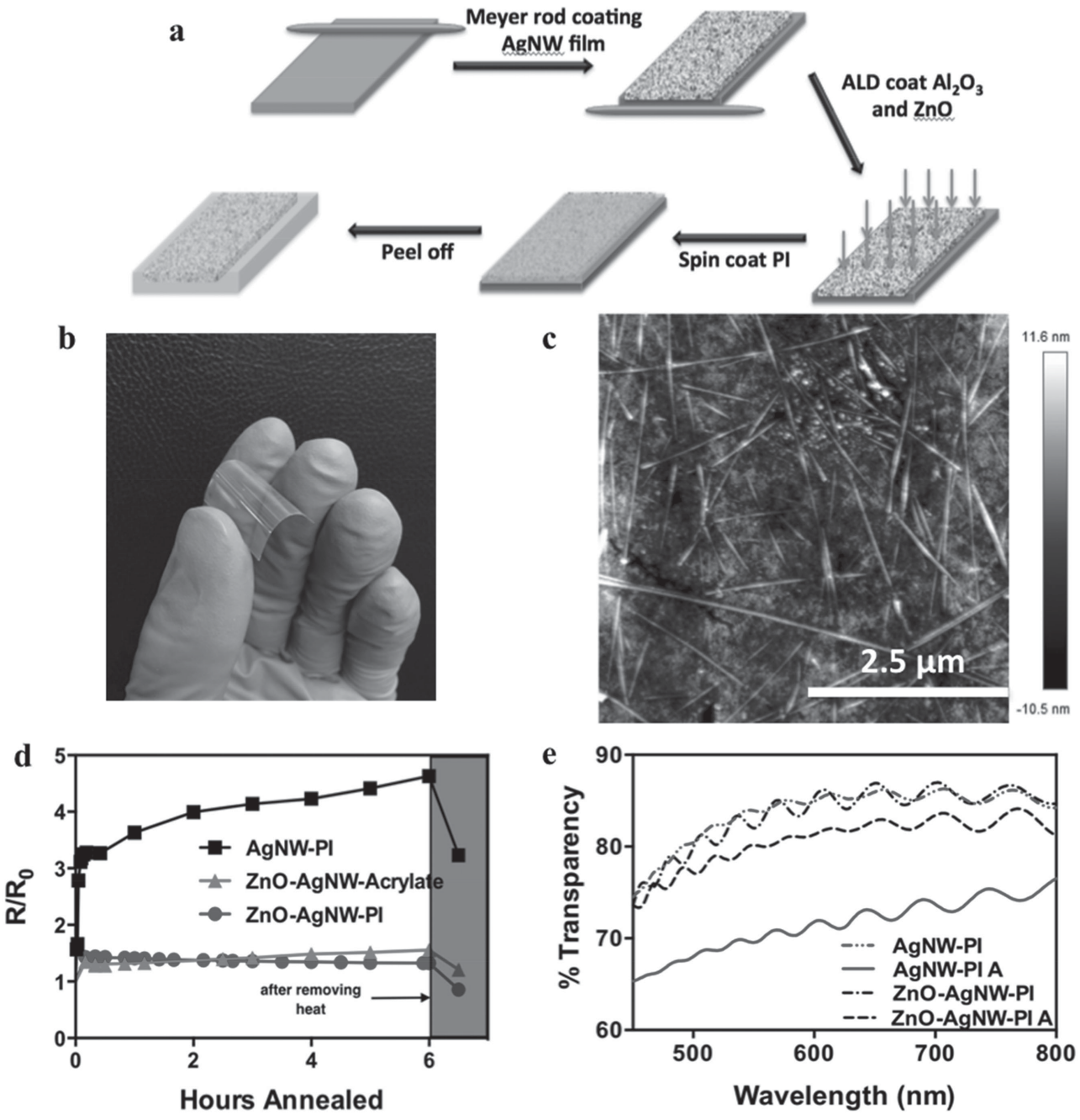

Figure 4. a) Fabrication process for a freestanding ZnO-AgNW-PI film. b) Optical image of a ZnO-AgNW-PI composite electrode. c) AFM image of embedded ZnO-AgNW-PI substrate. d) Normalized sheet resistance of the ZnO-AgNW-PI heated at 300 °C, and two reference electrodes annealed at 250 °C as a function of hours annealed. e) UV–vis spectra of ZnO-AgNW-PI film annealed at 300 °C for 1 h and AgNW-PI film at 250 °C for 1 h.

resistance. The AgNW-PI electrode was also tested at 300 °C, where similar to the AgNW-acrylate films, the electrode failed to register a resistance within a few minutes. In contrast, the ZnO coated films showed significantly better electrical performance, with the ZnO-acrylate electrode increasing in sheet resistance by only 21%, and the ZnO-AgNW-PI decreasing in sheet resistance by 15%. This decrease in sheet resistance is attributed to the fusing of nanowires at the junction, as the high annealing temperature allows the noncoated regions at the point of intersection of the nanowires to melt and fuse together, while the outer ZnO shell prevents the complete melting of the nanowires. The fusing of nanowires at the junction lowers the junction resistance of the nanowires, which in turn, lowers the overall sheet resistance of the electrode.

In addition to the electrical stability, the ZnO-AgNW-PI electrode was also able to withstand the 6 h anneal at 300 °C without significant optical deterioration of the films, as seen in the UV–vis spectra in Figure 4e. Figure 4e illustrates a control

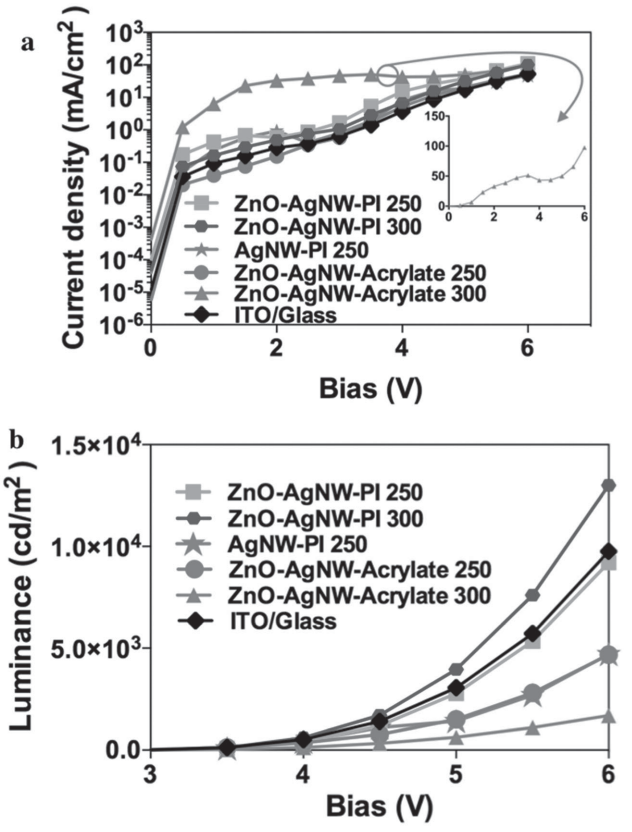

Figure 5. a) Current density as a function of voltage for various substrates annealed at 250 and 300 °C. ITO is annealed at 300 °C. PLED based on ZnO-AgNW-Acrylate heated at 300 °C is shown in the inset on a linear scale. b) Luminance as a function of voltage for the PLED devices with various substrates annealed at 250 and 300 °C. ITO is annealed at 300 °C.

AgNW-PI electrode before and after heating at 250 °C, along with the ZnO-AgNW-PI electrode before and after heating at 300 °C to demonstrate the efficacy of ZnO in preventing oxidation of the nanowires within the PI polymer matrix. The wave-like characteristics of the spectrum are characteristic of the PI polymer.[36] For the pristine AgNW embedded within the PI matrix, a 14.4% decrease in transparency is observed before and after heating at 250 °C, in contrast to a 1.9% loss in transparency in the ZnO-AgNW-PI freestanding electrode after heating at 300 °C. AgNW-acrylate and ZnO-AgNW-acrylate electrodes were also analyzed before and after heating at 250 °C to highlight the thermal resistance of the PI substrate. The acrylate substrate exhibited significant yellowing of the film, quantified by a 31% transparency loss for the ZnO-AgNW-acrylate electrode, and a 43% loss for the pristine AgNW-acrylate electrode. This yellowing in the acrylate is a deterioration often observed in plastic films due to radical-activated oxidative degeneration of the hydrocarbon backbone in the polymer material.[37]

To demonstrate the viability of the ZnO-AgNW-PI film as a flexible TCE, solution-processed white PLEDs were fabricated in a typical bottom-emissive structure. Solution processed bis(acetylacetonato) dioxomolybdenum(VI) [$MoO_2(acac)_2$] was used as the precursor for the hole injection layer, and was seen empirically from thermogravimetric analysis (TGA) and X-ray photoelectron spectroscopy (XPS) to require a minimum temperatures of 250 °C to begin the conversion to MoO_x. This solution processed MoO_x (s-MoO_x) has been reported as an effective hole-injection material to enhance hole injection in OLEDs and hole collection in organic photovoltaic cells.[38,39] A White Polymer (WP) from Cambridge Display Technology blended with 1,3-bis[(4-*tert*-butylphenyl)-1,3,4-oxidiazolyl)phenylene (OXD-7) was used for the emissive layer, with cesium fluoride and aluminum evaporated for the electron injection layer and cathode, respectively. Further detailed procedures of materials for the s-MoO_x and the PLED fabrication processes are described in the Experimental Section. The white PLEDs were fabricated on five different substrates: a ZnO-AgNW-PI hybrid electrode; a ZnO-AgNW-acrylate electrode; a pristine AgNW-PI electrode, the pristine AgNW-acrylate electrode used in our previous paper;[14] and sputtered ITO on a glass substrate. All polymer based electrodes were analyzed after heating the $MoO_2(acac)_2$ precursor both at 250 and 300 °C. Characteristic current density (J-V) and luminance-voltage curves are shown in **Figure 5**a,b, respectively. Data for PLEDs based on the pristine AgNW-acrylate electrode at both temperatures, in addition to the pristine AgNW-PI electrode at 300 °C are not shown as no light could be observed from these devices due to the immeasurably high resistance of the electrodes as discussed above. For the ZnO-AgNW-PI electrode, enhanced luminance at the higher annealing temperature was observed due to the formation of Mo^{4+} and Mo^{5+} species at higher temperatures. These reduced species lead to the formation of gap states in MoO_x, lowering the potential barrier height in contrast to what is expected from the phenomenological model, and in turn, enhancing PLED performance at devices annealed at higher temperatures and longer annealing times. The PLED based on the AgNW-PI electrode annealed at 250 °C was capable of light emission, though an increased resistance and decreased transparency resulted in a 63.7% lower luminance at 6 V as compared to the ZnO-AgNW-PI annealed at 300 °C. ZnO-AgNW-acrylate based diodes were capable of light emission at both annealing temperatures, though significant transparency loss for both samples annealed at 250 and 300 °C resulted in a 64.0% and 87.0% luminance loss at 6 V, respectively in contrast with the ZnO-AgNW-PI based diode. Furthermore, with higher annealing temperatures, the presence of localized shorts in the devices was observed, as seen in the inset of Figure 5a. These shorts in the device may also contribute to the lower luminance, as illustrated in Figure 5b. The ZnO-AgNW-PI electrode annealed at 300 °C exhibited similar luminance to ITO using the same device structure and processing conditions. The maximum external quantum efficiency (EQE) and current efficiency (CE) for ITO based devices was 7.7% and 14.7 cd A^{-1}, while corresponding efficiencies for the ZnO-AgNW-PI PLED was 6.9% and 13.2 cd A^{-1}. All other EQEs and CEs for PLEDs based on reference electrodes were under 5% and 10 cd A^{-1}, respectively. The comparable performance of the ZnO-AgNW-PI PLED and ITO/glass PLED with the same processing condition verifies the new composite substrate's efficacy for use in optoelectronic devices requiring high processing temperatures. It is expected that significantly improved performance can further be obtained with the dispersion of nanoparticles within the polymer matrix to enhance light extraction.[14] We anticipate that the ZnO-AgNW-PI composite electrode can be used for

emerging flexible optoelectronic devices requiring high temperature fabrication processing in a transition away from conventional TCE materials.

3. Conclusion

A TCE has been fabricated for high performance optoelectronic devices requiring high processing temperatures. The TCE is comprised of AgNW coated with a thin, conformal layer of ZnO deposited with ALD, embedded within a PI matrix. Enhanced thermal stability based on electrical and optical performance of the ZnO coated AgNW film was observed. The freestanding ZnO-AgNW-PI film also showed excellent thermal stability in regards to both electrical and optical performance. Because the high temperature stable AgNWs are embedded within the PI, the resulting TCE has a smooth surface topography, allowing its use for optoelectronic devices requiring smooth interfaces. As proof of viability, a white PLED was fabricated on the ZnO-AgNW-PI film comprising a layer of MoO_x processed from solution followed by annealing at 250 or 300 °C. The PLED exhibited comparable performance to controls on ITO/glass, and vastly outperforming control devices with one or no thermally stable component (ZnO and PI). The ZnO-AgNW-PI electrode shows great promise for replacing ITO as it ameliorates two significant limitation of flexible, plastic TCEs hindering their widespread adoption —low thermal stability and high surface roughness.

4. Experimental Section

Materials: GO was prepared from graphite by the modified Hummers method.[40] AgNWs were purchased from Zhejiang Kechuang Advanced Materials Co., LTD. PI was obtained from Nexolve Materials. 2,2-Dimethoxy-2phenylacetophenone (photoinitator), anhydrous chlorobenzene, chlorobenzene, and bis(acetylacetonato) dioxomolybdenum(VI) were obtained from Sigma-Aldrich. PEDOT:PSS (Clevios VP AL4083) was purchased from H.C. Starck Inc. Zonyl FS-300 fluorosurfactant was purchased from Fluka Analytical. A white-light-emitting polymer (WP) was provided by Cambridge Display Technology, and 1,3-bis[(4-tert-butylphenyl)-1,3,4-oxidiazolyl)phenylene (OXD-7) was obtained from Lumtech.

Preparation of ZnO-AgNW Networks and Freestanding ZnO-AgNW-PI Composite Electrodes: GO powder was dispersed in deionized (DI) water at a concentration of 2 mg mL^{-1} in an ultrasonic bath for 15 min. The resulting solution was further diluted with isopropyl alcohol (IPA) to 0.2 mg/5 mL, and sonicated for 15 min before use. A glass slide was placed flat, and the solution of GO drop-casted into a thin line at the top of glass and drawn down with a Meyer rod. The resulting films were annealed on a hot plate at 150 °C for 30 min. Subsequently, AgNW solution was drawn down on the GO covered glass slide prior to annealing at 150 °C for 3 min, soaking in DI water for 10 min, and a second annealing at 165 °C for 8 min. GO-AgNW slides were introduced into a Fiji ALD chamber from Cambridge NanoTech. Al_2O_3 was deposited at 100 °C from TMA and H_2O precursors, with pulse and purge times for the two precursors both being 0.06 and 30 s. ZnO was deposited at 100 °C following Al_2O_3 deposition from $(C_2H_5)_2Zn$, diethyl zinc (DEZ), and H_2O, with pulse times for the two precursors being 0.06/45 s, and 0.06/60 s, respectively.

PI solution was made by dissolving 20% PI in chlorobenzene. The soluble PI was spun onto the ZnO-AgNW or bare AgNW coated glass before peeling off.

Fabrication of White PLED: In a typical procedure for ZnO-AgNW-PI electrode based devices described, freestanding electrodes were cleaned in an ultrasonic bath with detergent and DI water for 30 min, before being soaking and rinsing with ethanol. A solution of 0.3 wt% $MoO_2(acac)_2$ in IPA was spin-coated on the substrate at 2000 rpm for 60 s, and then annealed at 250 °C or 300 °C for 1 h. The films were next spun with a solution of 2000:1 vol% (PEDOT:PSS):(Zonyl FS-300) at 1100 rpm for 30 s, followed by annealing at 130 °C for 30 min to dry off any residual solvent. The white polymer emissive layer was spun from a solution of 100:10 wt% WP:OXD-7 in chlorobenzene. A 1 nm layer of cesium fluoride (CsF) and 100 nm of aluminum (Al) were evaporated onto the substrate through a shadow mask at 10^{-6} Torr.

Characteriztion Methods: Scanning electron microscopy (SEM) was performed on a JOEL JSM-6701F scanning electron microscope. Transmittance spectra were obtained with a Shimadzu UV-1700 spectrophotometer. Surface topography was carried out on a Dimension Icon Scanning Probe Microscope (SPM) from Bruker. Electrical measurements for the white PLED were carried out in a nitrogen atmosphere glovebox, with the current and light voltage curves being measured with a Keithley 2400 source meter and calibrated silicon photodetector by sweeping the applied voltage from 0 to 6 V at 500 mV increments per step. All characterization tests were carried out at room temperature.

Supporting Information

Supporting Information is available from the Wiley Online Library or from the author.

Acknowledgements

The work was supported by NSF award number IIP-1414415. The authors acknowledge the use of instruments at the Nano and Pico Characterization Lab at the California NanoSystems Institute. The authors acknowledge the use of instruments at the Electron Imaging Center for NanoMachines supported by NIH (1S10RR23057 to Z.H.Z.) and CNSI at UCLA. The authors acknowledge and thank W. Lin of the UCLA Nanoelectronics Research Facility for assistance and discussion on ALD processing.

Received: August 3, 2015
Revised: September 19, 2015
Published online: November 10, 2015

[1] L. Hu, H. Wu, Y. Cui, *MRS Bull.* **2011**, *36*, 760.
[2] A. Kumar, C. Zhou, *ACS Nano* **2010**, *4*, 11.
[3] T. Hamaguchi, K. Omae, T. Takebayashi, Y. Kikuchi, N. Yoshioka, Y. Nishiwaki, a. Tanaka, M. Hirata, O. Taguchi, T. Chonan, *Occup. Environ. Med.* **2008**, *65*, 51.
[4] Z. Chen, *Thin Solid Films* **2001**, *394*, 201.
[5] K. Ellmer, *Nat. Photonics* **2012**, *6*, 808.
[6] M. W. Rowell, M. a. Topinka, M. D. McGehee, H. J. Prall, G. Dennler, N. S. Sariciftci, L. Hu, G. Gruner, *Appl. Phys. Lett.* **2006**, *88*, 86.
[7] D. Zhang, K. Ryu, X. Liu, E. Polikarpov, J. Ly, M. E. Tompson, C. Zhou, *Nano Lett.* **2006**, *6*, 1880.
[8] K. S. Kim, Y. Zhao, H. Jang, S. Y. Lee, J. M. Kim, K. S. Kim, J.-H. Ahn, P. Kim, J.-Y. Choi, B. H. Hong, *Nature* **2009**, *457*, 706.
[9] S. Bae, H. Kim, Y. Lee, X. Xu, J.-S. Park, Y. Zheng, J. Balakrishnan, T. Lei, H. R. Kim, Y. Il Song, Y.-J. Kim, K. S. Kim, B. Ozyilmaz, J.-H. Ahn, B. H. Hong, S. Iijima, *Nat. Nanotechnol.* **2010**, *5*, 574.
[10] J. Zou, H. L. Yip, S. K. Hau, A. K. Y. Jen, *Appl. Phys. Lett.* **2010**, *96*, 3.
[11] M. Song, J. H. Park, C. S. Kim, D.-H. Kim, Y.-C. Kang, S.-H. Jin, W.-Y. Jin, J.-W. Kang, *Nano Res.* **2014**, *7*, 1370.

[12] J. Liang, L. Li, X. Niu, Z. Yu, Q. Pei, *Nat. Photonics* **2013**, *7*, 817.
[13] H.-G. Im, J. Jin, J.-H. Ko, J. Lee, J.-Y. Lee, B.-S. Bae, *Nanoscale* **2014**, *6*, 711.
[14] L. Li, J. Liang, S.-Y. Chou, X. Zhu, X. Niu, Zhibin Yu, Q. Pei, *Sci. Rep.* **2014**, *4*, 4307.
[15] H. Im, S. Jung, J. Jin, D. Lee, J. Lee, D. Lee, J. Lee, *ACS Nano* **2014**, *8*, 10973.
[16] X. Y. Zeng, Q. K. Zhang, R. M. Yu, C. Z. Lu, *Adv. Mater.* **2010**, *22*, 4484.
[17] J. Li, J. Liang, X. Jian, W. Hu, J. Li, Q. Pei, *Macromol. Mater. Eng.* **2014**, *299*, 1403.
[18] Z. Yu, L. Li, Q. Zhang, W. Hu, Q. Pei, *Adv. Mater.* **2011**, *23*, 4453.
[19] Q. Huang, W. Shen, X. Fang, G. Chen, Y. Yang, J. Huang, R. Tan, W. Song, *ACS Appl. Mater. Interfaces* **2015**, *7*, 4299.
[20] J. Y. Lee, S. T. Connor, Y. Cui, P. Peumans, *Nano Lett.* **2008**, *8*, 689.
[21] J. Chen, H. Ahn, S. Yen, Y. Tsai, *ACS Appl. Mater. Interfaces* **2014**, *6*, 20994.
[22] A. Kim, Y. Won, K. Woo, C. H. Kim, J. Moon, *ACS Nano* **2013**, *7*, 1081.
[23] Q. Xu, W. Shen, Q. Huang, Y. Yang, R. Tan, K. Zhu, N. Dai, W. Song, *J. Mater. Chem. C* **2014**, *2*, 3750.
[24] S. Chen, L. Song, Z. Tao, X. Shao, Y. Huang, Q. Cui, X. Guo, *Org. Electron.* **2014**, *15*, 3654.
[25] M. Göbelt, R. Keding, S. W. Schmitt, B. Hoffmann, S. Jäckle, M. Latzel, V. V. Radmilović, V. R. Radmilović, E. Spiecker, S. Christiansen, *Nano Energy* **2015**, *16*, 196.
[26] S. D. Standridge, G. C. Schatz, J. T. Hupp, *Langmuir* **2009**, *25*, 2596.
[27] Z. Ji, X. Shen, M. Li, H. Zhou, G. Zhu, K. Chen, *Nanotechnology* **2013**, *24*, 115603.
[28] A. V. Whitney, J. W. Elam, P. C. Stair, R. P. Van Duyne, *J. Phys. Chem. C* **2007**, *111*, 16827.
[29] G. Guisbiers, S. Pereira, *Nanotechnology* **2007**, *18*, 435710.
[30] I. Perez, E. Robertson, P. Banerjee, L. Henn-Lecordier, S. J. Son, S. B. Lee, G. W. Rubloff, *Small* **2008**, *4*, 1223.
[31] H. Y. Lee, C. J. An, S. J. Piao, D. Y. Ahn, M. T. Kim, Y. S. Min, *J. Phys. Chem. C* **2010**, *114*, 18601.
[32] T. Bin Song, Y. Chen, C. H. Chung, Y. Yang, B. Bob, H. S. Duan, G. Li, K. N. Tu, Y. Huang, *ACS Nano* **2014**, *8*, 2804.
[33] M. Zhao, X. H. Zhou, Q. Jiang, *J. Mater. Res.* **2001**, *16*, 3304.
[34] J. L. Elechiguerra, L. Larios-Lopez, C. Liu, D. Garcia-Gutierrez, A. Camacho-Bragado, M. J. Yacaman, *Chem. Mater.* **2005**, *17*, 6042.
[35] S. Sorel, P. E. Lyons, S. De, J. C. Dickerson, J. N. Coleman, *Nanotechnology* **2012**, *23*, 185201.
[36] C. P. Ennis, R. I. Kaiser, *Phys. Chem. Chem. Phys.* **2010**, *12*, 14884.
[37] S. Yang, S.-Y. Kwak, J. Jin, J.-S. Kim, Y. Choi, K.-W. Paik, B.-S. Bae, *J. Mater. Chem.* **2012**, *22*, 8874.
[38] K. Zilberberg, H. Gharbi, A. Behrendt, S. Trost, T. Riedl, *ACS Appl. Mater. Interfaces* **2012**, *4*, 1164.
[39] M. Takayama, S. Naka, H. Okada, *Jpn. J. Appl. Phys.* **2013**, *52*, 1.
[40] D. A. Dikin, S. Stankovich, E. J. Zimney, R. D. Piner, G. H. B. Dommett, G. Evmenenko, S. T. Nguyen, R. S. Ruoff, *Nature* **2007**, *448*, 457.